2023 IEEE International Conference on Robotics and Automation (ICRA 2023)
May 29 - June 2, 2023. London, UK

Tactile Identification of Object Shapes via In-Hand Manipulation with A Minimalistic Barometric Tactile Sensor Array

Xin Zhou, *Student Member, IEEE, and* Adam J. Spiers, *Member, IEEE*

***Abstract*—With the goal of providing an alternative to optical and other tactile sensors, we set out to stress test the object shape identification capabilities of barometric tactile arrays in robotic manipulation tasks. These sensors are superior to optical devices in terms of form factor, ease of fabrication, and data reading/processing speeds, but lack the necessary spatial resolution to identify surface shapes via a single contact. To compensate, we utilize in-hand-manipulation, specifically in-hand-rolling to identify object shapes via a spatiotemporal approach. To increase task difficulty, we only use three neighboring barometric sensors and designed strict experiment requirements with the purpose of creating a set of extremely confusable test objects. The E-TRoll robotic hand, equipped with a barometric tactile array on one finger, was used to roll test objects within its grasp, taking just under 3.4 seconds for data collection under the fastest tested speed setting, compared to 33 seconds in our previous work. We also designed and implemented a feature extraction algorithm, based and improved upon our recently published algorithm. This captures enough information from the collected spatiotemporal data samples for successful classification with only 13 features. Finally, a bagged tree classification algorithm was trained and optimized with data from 1,164 trials of rolling 9 prismatic test objects, leading to a five-fold cross validation accuracy of 90.5% for identifying the 9 object classes.**

I. Introduction

In recent years, tactile sensing has been recognized as an important perceptual modality for robotic manipulation. To ensure safe and compliant object grasping, methods of force feedback [1], slip detection [2]–[4], and object stiffness estimation [5] have been widely researched and applied to real-world tasks. However, researchers are still looking for robust and efficient (both financially and computationally) tactile solutions to aid active object manipulation beyond the less complex task of safe grasping.

In particular, the identification of surface shapes has been frequently investigated [6]–[9], not without good reason. Beyond the identification of unknown objects/features in scenarios where cameras fail, object-contour knowledge can be used for additional manipulation tasks. A human example is unlocking a door in the dark. A brief exploration by touch can tell us which part of a key must be inserted into a lock and which part of the key should be grasped.

Several optical tactile sensors are currently in use by robotics researchers to perform shape detection – including the TacTip [10], Gelsight [1], and DIGIT sensors [11]. Note that DIGIT is based on the same sensing principle as Gelsight and is effectively an improved open-source version of it. All of them utilize an optical camera to estimate deformations in a malleable sensing surface. Multiple well-cited pieces of work such as [7], [12], [13] have used those sensors to estimate local surface shapes due to their simplicity: a single press against an object surface is sufficient. Nevertheless, these optical sensors have common drawbacks, namely their bulkiness, limited sensing surface size, and slow speeds due to the need of processing large visual images.

Figure 1: The E-TRoll hand has two rotary joints and a prismatic palm, with a barometric tactile array mounted on one of the two fingers. The orange test object is automatically lifted to the desired height for rolling.

We believe that another lesser researched open-source tactile sensor deserves more attention: tactile array sensors based on commercial MEMs barometers [14]. These tactile sensors are low cost, easy to fabricate, and most importantly only have a thickness of a few millimeters, all whilst having an easily extendable sensing surface and much faster speeds due to each barometer only outputting a single reading at a time. These desirable features make them easily mountable on existing robot hands and fast enough to complement existing robotic manipulation approaches. Naturally, the fast speed comes at the cost of sensing resolution. The (no longer commercially available) TakkTile barometric tactile sensors used in this paper have a sensor-center spacing of 8 mm, which is too large to estimate small surface shapes through a single contact. Even with the recently emerged superresolution techniques by Sun et al. [15] (which can improve resolution 1200-fold), local shape features cannot be estimated based on a single press, as Sun's technique can only be applied to single-point contacts.

To enable local shape identification with low-resolution barometric tactile arrays, we abandon single-press approaches and opt for in-hand manipulation, namely rolling between the fingers of the E-Troll gripper [16] as shown in Fig. 1.

* Research supported by Imperial College London internal funds.
Both authors are with Imperial College London (corresponding author: xin.zhou16@imperial.ac.uk).

By rolling prismatic objects between two fingers, small polygonal prisms with varying number of base sides (hence varying edge angles) as well as small cylinders of varying radii were successfully identified with success rates of 90.5%. This was achieved with only three barometers spaced at 8 mm. In-hand rolling also has significant benefits in terms of completion time. Whilst single-press approaches typical of optical tactile sensors analyze only a small surface area at a time with the need to reposition the sensing surface repeatedly [7], [17], in-hand rolling can expose a whole sliced section of an object via a swift and simple rolling action while grasping the object. For context, Chu et al. performed one contact action within roughly 4 seconds to expose a finger-tip sized area to a BioTac sensor [17], whereas one full rolling action in our experiments can be performed under 3.4 seconds and covers an area of approximately 3 times the size (if all sensors were active).

This work builds upon our previously published paper [16], which also investigates the task of object shape identification using the same hand and same sensors. However, whilst our previous work was a proof-of-concept for shape identification, this paper stress tests the system with a significantly harder classification task: Only a fingertip sized sensing surface is used which is more than 3 times smaller than in the previous work; Rolling is completed in more than an order of magnitude less time resulting in more than an order of magnitude fewer readings per collected spatiotemporal data sample; And finally, strict experiment requirements for test object design and data processing methods lead to a set of remarkably more mistakable test objects.

II. System Overview

A. MEMs Barometer Based Tactile Sensors

The tactile sensors used in this work are fabricated by RightHand Robotics, Inc. under the product name TakkStrip 2 [18]. Within the Takkstrip 2, six MPL115A MEMs barometers are aligned in a single row on a PCB board with an 8 mm spacing between the center of adjacent sensors. All barometers are cast in a single 3.5 mm thick layer of VytaFlex 20 urethane rubber, sold by Smooth-On, Inc. (Fig. 2). Although the TakkStrip 2 sensors are no longer commercially available, the design is open-source and is based on the sensing principle described in [14]. For our experiments, three adjacent barometers were active, resulting in a fingertip-sized sensing surface with an estimated length of 24 mm.

B. Gripper Design

The E-TRoll (Enhanced-Tactile Rolling) robotic gripper used in this work was designed by us for rolling tasks and described in detail in [16]. To summarize, the hand consists of two single-linkage fingers with a rotary joint at each finger's base. The joints are directly driven by a Dynamixel XM430-W350-R servo motors. Another servo motor of the same model uses a double rack-and-pinion mechanism to dynamically vary the distance between the two finger bases, effectively creating a variable width palm (Fig. 1). All structural parts were 3D printed on a Raise3D E2 printer using Raise3D PLA filaments. Two Takkstrip 2 sensors are mounted back-to-back on one of the two fingers (the sensing finger), virtually creating a single row of 12 barometric sensors. Although as already mentioned, for the purpose of this work

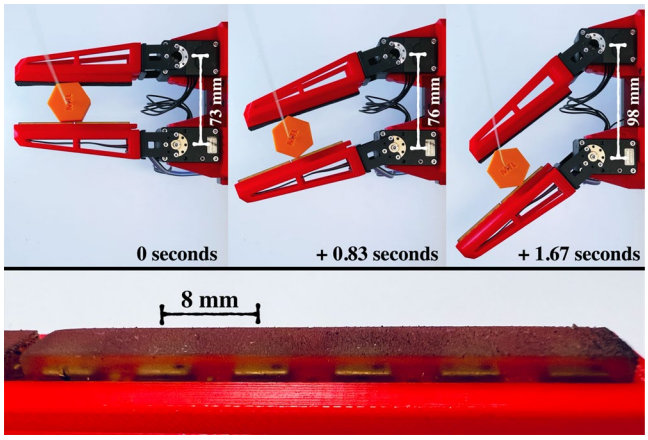

Figure 2: (Top) The E-TRoll gripper rolls a hexagonal prism along the sensing finger. Note how the dynamic palm adjusts its width during rolling to keep the two fingers parallel. (Bottom) Close up view of the barometric tactile array with 8 mm between each adjacent sensor centers.

only three barometers were active. During object rolling (Fig. 2), the servo motor for the sensing finger is set in position control mode, whilst the other finger (the 'pushing finger') is under current control mode, effectively applying a constant torque towards the sensing finger to tightly clamp the object. The variable width palm dynamically adjusts the palm width to keep the two fingers parallel to one another during rolling, which typically extends the rolling range (in degrees) compared to fixed finger bases (as in [9]) by over 100%. The dynamically parallel finger arrangement also ensures that the force applied by the pushing finger onto the object is always perpendicular to the sensing finger. More details on the involved control system can be found in [16].

C. Semi-Automated Data Collection Rig

For the experiments conducted in this work, each test object was rolled 150 times, introducing significant manual

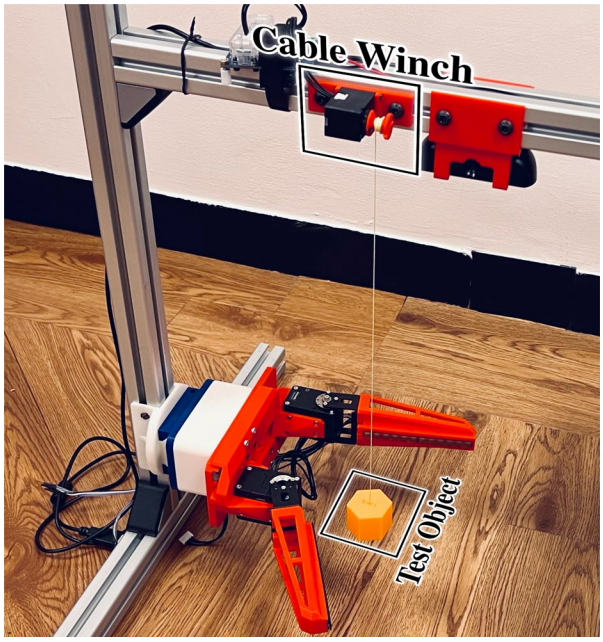

Figure 3: The cable winch is used to initialize the test object's height and randomize its position and orientation.

labor for resetting the test objects to their initial positions. Hence a semi-automated test rig was built to reset the object position after each rolling task. Note that this rig is not fully automatic, as manual labor is still required to attach a new test object after 150 experiment runs are completed.

As can be seen in Fig. 3, the robotic gripper is mounted on a metal frame built with generic and widely available 30 × 30 mm extruded aluminum struts. A budget (£25) Dynamixel XL330-M288-T servo motor is mounted on the horizontal strut above the hand as a cable winch. The 3D printed winch drum is directly mounted to the servo horn. A long string is tied onto the winch drum and connected to the test object. After every rolling experiment run, the hand releases the object, upon which the winch activates, lifting the object from its final position. It then releases, placing the object back down at the starting position. The next experiment run starts with the hand grasping the object, followed by the winch releasing around 10 cm of string to allow unaffected rolling, and finally ending with the main rolling procedure.

For our experiments, it is essential that the starting positions as well as orientations are randomized, so the string is attached to the center of the top base of each prismatic test object to allow free rotation around the primary axis of the object. Furthermore, when the object is freely suspended on the string between experiment runs, a small amount of desirable swinging is always present to randomize the starting position along the sensing finger within a range of roughly 20 mm.

III. Methods

A. Experiment Setup

The goal of the experiment is to investigate whether a limited number of low-resolution barometric tactile sensors can identify small surface shape features when combined with in-hand rolling and machine learning techniques. With only a small surface area of a rolled object exposed to the sensing surface, our classification model is tasked to identify objects solely based on tactile data.

TABLE I. Rolling Procedure

Step	Description
1	**Hand & object initialisation 1**: Both fingers set to position control mode. Sensing finger set to starting angle of -44°. Pushing finger set to -66° to allow space for the object. Palm width fixed at 65 mm. Object is now released if previously clamped between two fingers. Object set to the correct grasping height by the winch and is suspended freely between the two fingers.
2	**Hand & Object Initialisation 2:** Pushing finger switches to current control mode to push the object against the sensing finger at constant torque. Sensing finger kept at -44°. Palm width controller activated to keep both fingers parallel and force pushing finger to -44°.Winch releases about 10 mm of string to allow unaffected rolling. Rolling experiment run ready to begin.
3	**Main Experiment:** Pushing finger kept at current control mode for constant torque, tightly clamping the object during rolling. Sensing finger moves to +44° at constant angular velocity. Palm width controller active to keep fingers parallel. Tactile sensors collecting data at 31.1Hz.
4	**Return:** Stop data collection. Sensing finger moves back to the initial -44° with clamping and palm width controller active, effectively rolling the object back to near the initial position. This prevents the object from exessice swinging.

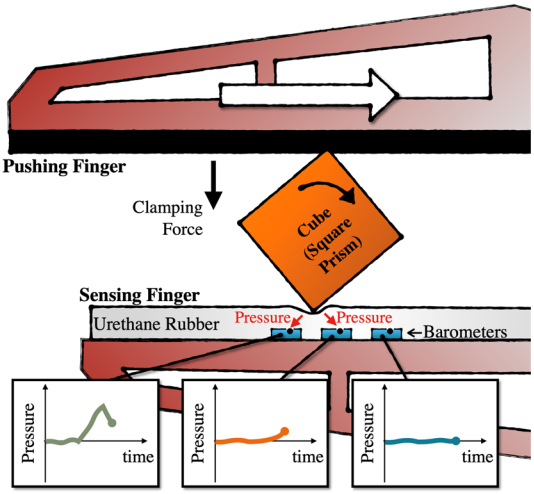

Figure 4: A simplified illustration of the E-TRoll hand rolling a cubic test object across the three active barometric sensors. With the sensing finger as the reference frame, the pushing finger moves to the right, rolling the cube clockwise. A clamping force keeps the object tightly pressed against the sensing surface, resulting in different pressure readings in each of the barometers. Note that the same colours are used to represent readings from the three barometers throughout this manuscript.

As illustrated in Fig. 4., the basic setup of the experiment is to roll various prismatic objects across the small sensing surface on the robotic finger. The rolling is performed by the hand described in section *II. System Overview* with the tactile data collected at a 31.1Hz sampling rate. All test objects are rolled at a constant angular velocity of the sensing finger with three speed settings. The reasoning for using varied speed settings is explained later in this section. For each of the 9 test objects, 50 experiment runs are conducted for each speed setting, resulting in a dataset of 1,350 spatiotemporal data samples. Each spatiotemporal data sample has a dimension of 3 (sensors) by either 205 ± 5 at low speed settings, 140 ± 3 at medium speed settings, or 106 ± 2 at high speed settings. Full rolling actions from a sensing finger angle of -44° to +44° takes just under 6.7 seconds, 4.5 seconds, and 3.4 seconds under low, medium, and high speed settings respectively. The procedure for each of the 1,350 experiment runs is outlined in Table I.

B. Experiment Design Requirements

Multiple strict design requirements are in place to increase the task difficulty. These requirements enable us to get a better understanding of how well our system generalizes across different object shapes.

1) Relative Timing Information

When comparing the tactile data from cylinders of 18 mm and 36 mm diameters, rolled at the identical speed setting (constant angular finger velocity), it becomes clear that cylinders with greater diameters travel faster along the sensing surface (Fig. 5A). This is due to a larger palm width during rolling. If any absolute time information was kept for classification (such as the width of each peak), the model would be able to distinguish prisms of various base diameters simply by their traversing velocities. Hence, all timing information must be relative to a temporal feature within the

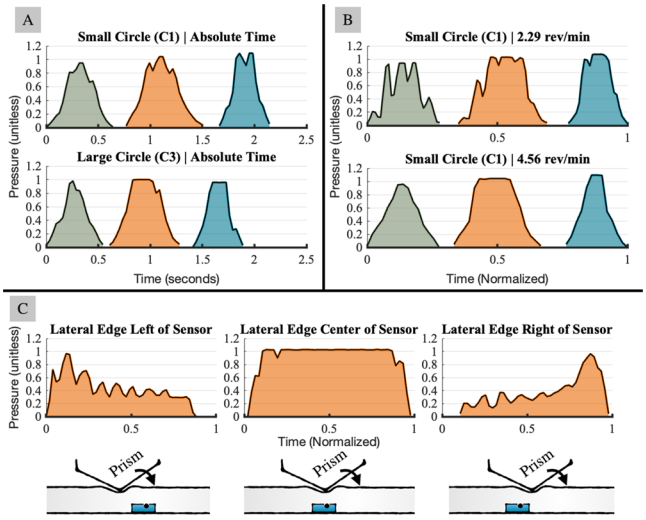

Figure 5: [A] Comparing the rolling of two differently sized cylinders at the same speed setting. [B] The same cylinder is rolled at two different speed settings with time normalized. [C] Comparing the response from one single sensor channel, when a polygonal prism's lateral edge presses against the sensing surface left, centre and right to the barometer.

same spatiotemporal data sample (such as taking the width of the first peak as a percentage of the second peak width).

2) Three Speed Settings

The sensing finger, which is in position control mode, is set at three different angular velocities during experiments: 2.29 rev/min, 3.435 rev/min, and 4.56 rev/min. Although all timing information is relative for classification, the sensing finger's angular velocity affects the collected tactile data as can be seen in Fig. 5B: As the sampling frequency is constant, lower rolling speeds provide a larger number of data points for each sensor channel's time series sample. However, lower speeds are also more prone to high frequency noise most likely introduced by small actuator oscillations from the dynamic palm's controller. Running experiments at different speed settings tests whether our classification method can deal with data of varying signal-to-noise ratios.

3) Identical Base Edge Lengths

The sensor response of contacting a polygonal prism's sharp lateral edge is highly dependent on the distance between contact point and sensor center, as shown in Fig. 5C. Hence, sensor readings hold positional information. To further (deliberately) increase the task difficulty, the polygonal test objects are designed to share the same base edge length. This way, during rolling, the prisms' lateral edges are exposed to the sensing surface at identical position intervals, making it impossible for the classification model to distinguish shapes simply based on positional information. Note that two sets of polygonal prisms are chosen, with the same base edge length within each set, but different ones between sets. This enables us to also investigate whether our system can distinguish objects based on base edge length (or more specifically the distance between lateral edge contacts).

4) Test Object diameter constraints

It is important that at least one lateral edge contacts the sensing surface during all rolling experiments. Hence each prism with a polygonal base cannot have a base edge

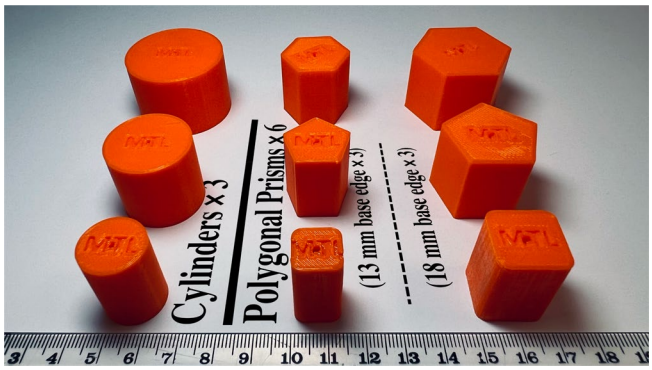

Figure 6: Photograph of all 9 Test objects, including 3 cylinders (left column), 3 polygonal prisms with a 13 mm base edge (middle column), and 3 polygonal prisms with an 18 mm base edge (right column).

exceeding the sensing surface length of 24 mm. Second, each barometer must be affected by no more than one edge contact, setting the minimum base edge length to around 8 mm. Third, the outer diameter of each base must not exceed 45 mm, otherwise the object might not cleanly fit between the two fingers at all times. And last, the minimum diameter of the circle inscribing the prism base (inner diameter) is set at 18 mm to ensure a travel distance along the sensing finger large enough to cover the whole of the sensing surface.

C. Objects & Data Collection

Nine test objects in total were used in this experiment – three cylinders (circular base), and two sets of polygonal prisms each consisting of one hexagonal prism, one pentagonal prism, and one square prism (cube) of identical base side lengths (Fig. 6). All objects were 3D printed on a Raise3D E2 printer using Raise3D premium PLA filament. Table II lists all test objects with their shape properties.

D. Data Preprocessing & Feature Extraction Algorithm

As the collected spatiotemporal tactile data has variable dimensions with a size of at least 3 × 104, using all datapoints for the classification model would introduce undesirably high model complexity. In addition, each sensor only outputs useful information upon contact with the test object, having a reading of 0 otherwise. This gives rise to the need for a feature extraction algorithm to capture the signal introduced by object contact via a small number of predefined features.

First, a Gaussian filter with a smoothing coefficient of 0.05 is applied to every sensor channel separately to eliminate most of the unwanted noise. For each time series in the three sensor

TABLE II. PRISMATIC TEST OBJECT PARAMETERS

Base Shape	Object ID	Side Length	Inscribed Circle Diameter	Circumscribed Circle Diameter
Circle	C1	NA	18.0	18.0
	C2	NA	27.0	27.0
	C3	NA	36.0	36.0
Square	S1	13.0	13.0	18.4
	S2	18.0	18.0	25.5
Pentagon	P1	13.0	17.9	22.1
	P2	18.0	24.8	30.6
Hexagon	H1	13.0	22.5	26.0
	H2	18.0	31.2	36.0

All Dimensions are in mm.

channels, the algorithm then extracts the useful part of the signal caused by object contact. This is achieved by starting from the timestamp at the maximum reading, then iterating both forwards and backwards in time until readings drop below 5% of the maximum value. The time series in between this range is then defined as a peak, if the maximum is larger than achievable by the noise leftover from the filtering. The noise is observed to be typically between ± 0.005 in our case, hence the threshold for a valid peak was chosen to be 0.01. Note that the readings in this experiment are not calibrated against any standard pressure units and are therefore unitless.

Only when three valid peaks are present, the data sample was deemed 'clean'. Otherwise the data sample was rejected. Out of the 1,350 collected samples, 1,164 samples (86.2%) were accepted. The remaining 186 samples all had peak maxima successfully exceeding the noise threshold (implying pressure measurements were sensed on each of the three sensors), but are incomplete due to the object not traversing the entirety of the sensing surface. This is caused by the starting position having too large a positional range during randomization, which suggests that the semi-automated testing rig needs to be improved in the future.

Fig. 7 presents a grid of selected peaks after Gaussian filtering. All three peaks for each presented experiment run (one for each sensor channel) are plotted on the same graph. Immediately noticeable from row 1 is how well-defined peaks from cylinders are compared to the peak plots from rolling polygonal prisms (rows 2–4). Furthermore, due to time normalization, the peaks from differently sized cylinders do not show any visible distinguishing trend or characteristics. Each row from rows 2–4 are peak plots collected from the same polygonal prism, but vary significantly within the same row. Some plots from different objects (e.g. H and L, or E and J, or F and I) are more similar to each other compared to other plots from their respective objects. These observations highlight the difficulty of the classification task.

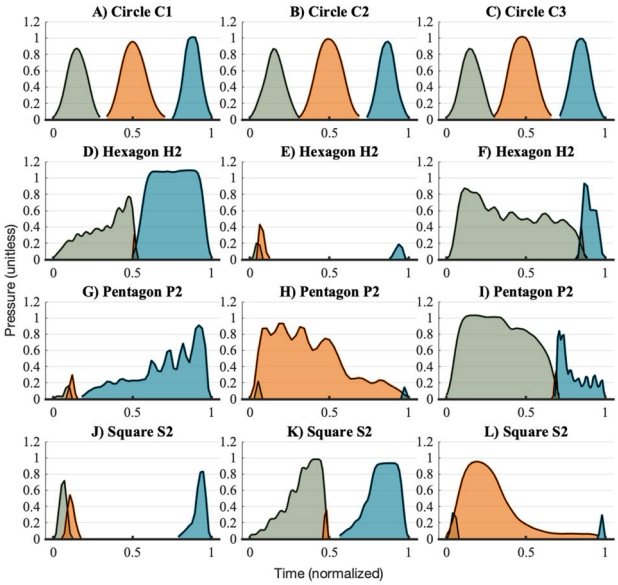

Figure 7: A selection of peak plots. Row 1 compares the three cylindrical test objects. Rows 2-4 present peak plots from rolling a large hexagonal, pentagonal, and square prism respectively. Times are normalized since no absolute timing information is allowed as per experiment requirements.

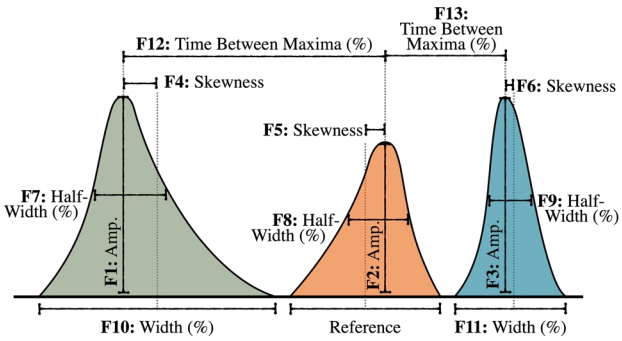

Figure 8: Visualization of the 13 Features (F1-F13) calculated by the feature extraction algorithm.

To distinguish the test objects, not only do we need to capture the shape, but also the timings of the three peaks. To capture shape, four parameters are of importance for each sensor channel: *amplitude*, which is simply the maximum reading during the peak; *width*, which is defined as the duration difference between the last reading and the first reading within the peak; *skewness*, calculated as the difference between time to the peak's mid-point and its maximum divided by peak width; and finally *half-width*, measured as the duration from when the peak first exceeds 50% of the amplitude to when it drops back below 50%. To capture the timing information of the three peaks, *time between maxima* is introduced, which simply calculates the time difference between the first and second, as well as second and third peak's maxima.

As specified by the experiment design requirements in Section *III.B Experiment Design Requirements*, only relative timing information is allowed to be kept as a predictor to eliminate dependence on rolling speed and object size. Hence, *width*, *half-width*, and *time between maxima* are calculated as a percentage of the second occurring peak's (sensor channel 2) *width*. Consequently, the second peak's *percentage width* is always 1 and is therefore not included as a feature.

The defined features are visualized in Fig. 8. In total, 13 final features were extracted for each 3-channel time series:

- F1, F2, F3: Amplitude
- F4, F5, F6: Skewness
- F7, F8, F9: Percentage half-width
- F10, F11: Percentage width
- F12, F13: Percentage time between maxima

E. Classification Model

The aim of the classification model is to distinguish various prismatic objects based on local surface shapes. Nine categories are defined for this task, one for each object. MATLAB's classification Learner tool was used to train a bagged trees model with Bayesian hyperparameter optimization. All 13 features from the feature extraction algorithm were used as input, and all 1,164 data samples were used to train the model. 5-fold cross-validation is used to validate the model accuracy.

IV. RESULTS

Overall, a 5-fold cross validation accuracy of 90.5% was achieved for classification of the nine objects. For context, we

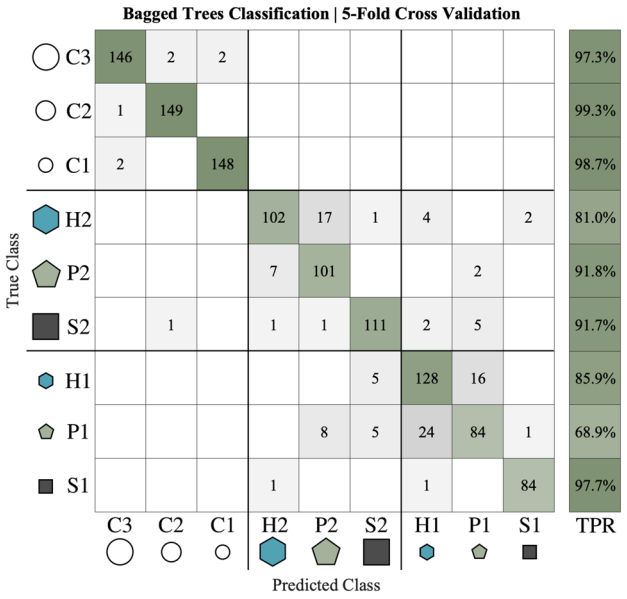

Figure 9: Confusion matrix for the five-fold cross-validation of the bagged trees classifier. The True Positive Rate (TPR) is presented as a separate column on the right. The 9 × 9 matrix is split into nine 3 × 3 segments (with thicker lines) to compare between the cylinder set, large polygonal prism set, and the small polygonal prism set. Object shapes are illustrated next to the object ID.

compare this piece of work with our previous work in [16] which uses the same hand and sensors for tactile shape identification. First, our previous work utilizes an 80 mm sensing surface (10 sensors) versus the 24 mm (3 sensors) used in this work. The previous work also rolls object over the sensing surface twice (once back and once forth) in around 33 seconds, whereas this work only requires a much faster single one-directional roll that can be performed under 3.4 seconds. Only 13 features are required to be captured in this work compared to the 80 features of the previous one. And most importantly, the previous work only classifies three easily recognizable objects (cylinder, square prism, and hexagonal prism) whereas the test objects in this work are designed to be purposefully mistakable. Yet, given the significantly harder classification task, much smaller feature vector size, radical reduction in required time, and less than third of the utilized sensing surface size, satisfactory classification results were achieved.

Three main factors made these performance improvements possible: Firstly, an adjusted feature extraction algorithm that, amongst other improvements, now also takes into account the half-width of a peak (or full width at half maximum) to distinguish between narrow peaks with long tails and wide peaks with short tails. Secondly, a more than ten-time increase in collected data samples. And lastly, an improved and optimized machine learning classification model.

Fig. 9 shows the confusion matrix for the 5-fold cross-validation results. First, it is noticeable that the classification model can almost perfectly tell apart polygonal prisms from cylinders. This is not surprising, given that rolling cylinders creates extremely well-behaved symmetrical peaks easily distinguishable from the seemingly unpredictable peaks generated by polygonal prims (comparing Fig. 7 A–C with D–L).

What is more surprising is the fact that cylinders of varying base diameters can be discriminated at such a high accuracy, with only 7 out of the 450 data samples being misclassified. Looking at Fig. 7 examples A to C, it is impossible to directly see any distinguishing features that can tell apart the sensor response from cylinders of the three different sizes. This suggests that machine learning approaches are essential for evaluating discreet surface shape features with low-resolution barometric sensors.

To investigate how well the model can distinguish different base edge lengths, we consider all observations within the center and bottom-right 3 × 3 segments in the confusion matrix as correct predictions, i.e., a small pentagon predicted as a small square still counts as correct, as the base edge lengths are identical. Out of the 714 observations from polygonal prisms, 679 (95.1%) have correctly identified base edge lengths. These results align with our previous findings in [16], where the model classifies three objects with varying base edges.

And finally, we investigate the model's ability to distinguish polygonal objects of the same base edge length. From the True Positive Rates (TPR), it is clear that pentagons and hexagons have the highest percentage of misclassified observations. In particular, distinguishing between the two shapes is difficult: Of the 45 and 47 misclassified hexagons and pentagons respectively, 33 (73.3%) and 31 (66.0%) are respectively predicted to be pentagons and hexagons. One explanation could be in the edge angles: there is a 18° angle difference between the corner of squares and pentagons, but only a 12° difference between that of pentagons and hexagons.

V. Conclusion

In this work, we have investigated whether, with the help of in-hand rolling and machine learning techniques, a small number of low-resolution barometric tactile sensors can identify object surface shapes that are challenging to identify via a single press against the sensor array. Multiple experiment requirements ensure that the nine test objects are extremely difficult to classify in order to stress test the sensors and the system. With a bagged tree classifier and a feature extraction algorithm, we achieved 90.5% 5-fold cross-validation accuracy, which is satisfactory given the task difficulty.

Our results indicate that the system can almost perfectly distinguish between even curvatures (cylinders) and shapes with corners (polygonal prisms), excellently identify object sizes (the radii of cylinders and the base edge lengths of polygonal prisms), and adequately differentiate between edge angles. Current results suggest a correlation between angle difference and prediction accuracy, but further experiments need to be conducted to quantify those findings.

We are planning on implementing object surface reconstruction/mapping via barometric tactile arrays and in-hand manipulation, which requires identification and localization of distinct surface features such as curvatures, sharp edges, and flat surfaces. In [15], Sun et al. already thoroughly quantified the excellent localization capabilities of these sensors. Now, through our findings, we are also confident that small surface features can be identified. We believe that our goal is now within reach.

REFERENCES

[1] W. Yuan, S. Dong, and E. H. Adelson, "GelSight: High-Resolution Robot Tactile Sensors for Estimating Geometry and Force," *Sensors*, vol. 17, no. 12, p. 2762, Nov. 2017, doi: 10.3390/S17122762.

[2] J. W. James and N. F. Lepora, "Slip detection for grasp stabilization with a multifingered tactile robot hand," *IEEE Transactions on Robotics*, vol. 37, no. 2, pp. 506–519, Apr. 2021, doi: 10.1109/TRO.2020.3031245.

[3] J. Reinecke, A. Dietrich, F. Schmidt, and M. Chalon, "Experimental comparison of slip detection strategies by tactile sensing with the BioTac® on the DLR hand arm system," *Proc IEEE Int Conf Robot Autom*, pp. 2742–2748, Sep. 2014, doi: 10.1109/ICRA.2014.6907252.

[4] J. W. James, N. Pestell, and N. F. Lepora, "Slip detection with a biomimetic tactile sensor," *IEEE Robot Autom Lett*, vol. 3, no. 4, pp. 3340–3346, Oct. 2018, doi: 10.1109/LRA.2018.2852797.

[5] Y. Zhang, Y. Mukaibo, and T. Maeno, "A multi-purpose tactile sensor inspired by human finger for texture and tissue stiffness detection," *2006 IEEE International Conference on Robotics and Biomimetics, ROBIO 2006*, pp. 159–164, 2006, doi: 10.1109/ROBIO.2006.340351.

[6] S. Luo, W. Mou, K. Althoefer, and H. Liu, "Novel Tactile-SIFT Descriptor for Object Shape Recognition," *IEEE Sens J*, vol. 15, no. 9, pp. 5001–5009, Sep. 2015, doi: 10.1109/JSEN.2015.2432127.

[7] S. Wang *et al.*, "3D Shape Perception from Monocular Vision, Touch, and Shape Priors," *IEEE International Conference on Intelligent Robots and Systems*, pp. 1606–1613, Dec. 2018, doi: 10.1109/IROS.2018.8593430.

[8] A. J. Spiers, M. v. Liarokapis, B. Calli, and A. M. Dollar, "Single-Grasp Object Classification and Feature Extraction with Simple Robot Hands and Tactile Sensors," *IEEE Trans Haptics*, vol. 9, no. 2, pp. 207–220, Apr. 2016, doi: 10.1109/TOH.2016.2521378.

[9] D. Mohtasham, G. Narayanan, B. Calli, and A. J. Spiers, "Haptic Object Parameter Estimation during Within-Hand-Manipulation with a Simple Robot Gripper," *IEEE Haptics Symposium, HAPTICS*, vol. 2020-March, pp. 140–147, 2020, doi: 10.1109/HAPTICS45997.2020.ras.HAP20.24.f5c34a19.

[10] B. Ward-Cherrier *et al.*, "The TacTip Family: Soft Optical Tactile Sensors with 3D-Printed Biomimetic Morphologies," *Soft Robot*, vol. 5, no. 2, pp. 216–227, Apr. 2018, doi: 10.1089/SORO.2017.0052.

[11] M. Lambeta *et al.*, "DIGIT: A Novel Design for a Low-Cost Compact High-Resolution Tactile Sensor with Application to In-Hand Manipulation," *IEEE Robot Autom Lett*, vol. 5, no. 3, pp. 3838–3845, May 2020, doi: 10.1109/LRA.2020.2977257.

[12] R. Li *et al.*, "Localization and manipulation of small parts using GelSight tactile sensing," *IEEE International Conference on Intelligent Robots and Systems*, pp. 3988–3993, Oct. 2014, doi: 10.1109/IROS.2014.6943123.

[13] N. F. Lepora, K. Aquilina, and L. Cramphorn, "Exploratory Tactile Servoing with Active Touch," *IEEE Robot Autom Lett*, vol. 2, no. 2, pp. 1156–1163, Apr. 2017, doi: 10.1109/LRA.2017.2662071.

[14] Y. Tenzer, L. P. Jentoft, and R. D. Howe, "The feel of MEMS barometers: Inexpensive and easily customized tactile array sensors," *IEEE Robot Autom Mag*, vol. 21, no. 3, pp. 89–95, Sep. 2014, doi: 10.1109/MRA.2014.2310152.

[15] H. Sun and G. Martius, "Guiding the design of superresolution tactile skins with taxel value isolines theory," *Sci Robot*, vol. 7, no. 63, p. eabm0608, Feb. 2022, doi: 10.1126/SCIROBOTICS.ABM0608/SUPPL_FILE/SCIROBOTICS.ABM0608_SM.PDF.

[16] X. Zhou and A. J. Spiers, "E-TRoll: Tactile Sensing and Classification via A Simple Robotic Gripper for Extended Rolling Manipulations," in *2022 IEEE/RSJ International Conference on Intelligent Robots and Systems (IROS)*, 2022.

[17] V. Chu *et al.*, "Using robotic exploratory procedures to learn the meaning of haptic adjectives," *Proc IEEE Int Conf Robot Autom*, pp. 3048–3055, 2013, doi: 10.1109/ICRA.2013.6631000.

[18] RightHand Labs, "TakkStrip 2." https://www.labs.righthandrobotics.com/takkstrip-2 (accessed Feb. 22, 2022).